Mookodi: multi-purpose low-resolution spectrograph and multi-filter photometric imager for rapid follow-up observations of astronomical transient events

Nicolas Erasmus[a,*] Iain A. Steele,[b] Andrzej S. Piascik,[b] Stuart D. Bates,[b] Chris. J. Mottram,[b] Kathryn A. Rosie[a] Carel H. D. R. van Gend,[a] Ulrich Geen,[a,c] Magaretha L. Pretorius,[a] Stephen B. Potter[a,d] Egan Loubser,[a] Willie Koorts,[a] Hitesh Gajjar,[a] Keegan Titus,[a] Hannah L. Worters,[a] Amanda A. Sickafoose[e] Sunil Chandra[a] James E. O'Connor,[a] Kgothatso Matlala[a] Justine Crook-Mansour[a] Ali Ranjbar,[b] Robert J. Smith,[b] Helen Jermak[b] Shalom Abiodun[a] and Okwudili D. Egbo[a,c]

[a]South African Astronomical Observatory, Cape Town, South Africa
[b]Liverpool John Moores University, Astrophysics Research Institute, IC2, LSP, Liverpool, United Kingdom
[c]University of Cape Town, Department of Astronomy, Cape Town, South Africa
[d]University of Johannesburg, Department of Physics, Johannesburg, South Africa
[e]Planetary Science Institute, Tucson, Arizona, United States

ABSTRACT. We present Mookodi (meaning "rainbow" in Sesotho), a multipurpose instrument with a low-resolution spectrograph mode and a multi-filter imaging mode for quick-reaction astronomical observations. The instrument, mounted on the 1-m Lesedi telescope at the South African Astronomical Observatory in Sutherland (South Africa), is based on the low-resolution spectrograph for the rapid acquisition of transients (SPRAT) instrument in operation on the 2-m Liverpool Telescope in La Palma (Canary Islands, Spain). Similar to SPRAT, Mookodi has a resolution $R \approx 350$ and an operating wavelength range in the visible ($\sim$4000 to 8000 Å). The linear optical design, as in SPRAT, is made possible through the combination of a volume phase holographic transmission grating as the dispersive element and a prism pair (grism), which makes it possible to rapidly and seamlessly switch to an imaging mode by pneumatically removing the slit and grism from the beam and using the same detector as in spectrographic mode to image the sky. This imaging mode is used for auto-target acquisition, but the inclusion of filter slides in Mookodi's design also provides the capability to perform imaging with a field-of-view $\approx 10' \times 10'$ ($\sim$0.6″/px) in the complete Sloan Digital Sky Survey filter set.

1 Introduction

Over the past decade, all-sky surveys such as Pan-STARRS,[1] Gaia,[2] Zwicky Transient Facility,[3] and Asteroid Terrestrial-impact Last Alert System[4] have provided a wealth of transient data of nearly the entire sky. Those surveys together reported $\sim$70,000 of the over 100,000 transients reported to the International Astronomical Union's Transient Name Server[5] (IAU TNS), since

---

*Address all correspondence to Nicolas Erasmus, n.erasmus@saao.nrf.ac.za

January 1, 2016.[6] However, the follow-up classification observations of these transient detections are sorely lagging behind with only ~13,000 classification spectra obtained of the transients identified by all surveys and reported to the TNS. The rate of transient discoveries and alerts will only increase exponentially in the next few years when even more data-intensive surveys, such as the Square Kilometre Array (SKA) project[7] in the radio and the Legacy Survey of Space and Time (LSST)[8] in the optical, are finally completed and fully operational. Although surveys such as The HUNt for Dynamic and Explosive Radio transients with meerKAT[9] (ThunderKAT) and TRansients And PUlsars with Meerkat[10] (TRAPUM) and dedicated transient surveys within the MeerKAT project[11] (a precursor array to SKA) are making radio-source transient discoveries, rapid follow-up in the visible wavelengths of any optical counterpart is still desirable to the scientific community.[12,13] This deluge of alerts expected in the very near future will only make the follow-up classification deficiency problem even worse.

The South African Astronomical Observatory (SAAO) has recently embarked on an initiative named the "Intelligent Observatory" or "IO" project.[14] One pillar of this project is to leverage the observatory's historic expertise in variable and time-domain astronomy and diverse instrument suites to facilitate more quick-reaction observations to transient alerts. The hope is to achieve this through greater integration of, robotic capability of, and external programmatic observation requests to the numerous telescopes (and instruments) owned and hosted at its observatory in Sutherland, Northern Cape, South Africa. The latest addition to the SAAO-owned telescopes on the plateau is the 1-m Lesedi telescope,[15] which is currently fully remotely operable and has fully robotic capability. This alt-azimuth mounted telescope has two Nasmyth ports with Sibonise (previous known as WiNCam[15]), a semi wide field multi-filter photometric imager, on the one port and now Mookodi, a low-resolution spectrograph and multi-filter photometric imager and the subject of this paper, on the other port. Both ports also have an auto-guider system fitted. The Lesedi telescope together with Mookodi is the first telescope-instrument combination to be integrated into the SAAO's IO project.

Mookodi is based on the existing low-resolution spectrograph for the rapid acquisition of transients (SPRAT) spectrograph[16] and designed and built by the Astrophysics Research Institute of Liverpool John Moores University (LJMU) following discussions in late 2017 between LJMU and the SAAO about the interest in such an instrument for the newly commissioned Lesedi telescope. As with SPRAT, one of Mookodi's main strengths is auto-target acquisition, which makes it a good fit for rapid-response spectroscopic follow-up observations via robotic observations, i.e., an ideal instrument for the SAAO's IO initiative. In addition to being a spectrograph, Mookodi has two significant alterations in comparison with SPRAT. The first is the use of a square detector (13.3 mm × 13.3 mm, 1024 px × 1024 px versus SPRAT's 26.6 mm × 6.6 mm, 1024 px × 255 px), and the second is the inclusion of two filter-slide mechanisms. These upgrades (especially the latter), with design input from the SAAO's instrumentation division, allows for the target acquisition mode of the instrument to also have the possibility to function as a multi-filter photometric imager for science exposures. This capability of rapidly switching between spectroscopy mode and photometric imaging mode also makes Mookodi an attractive instrument for the SAAO's IO initiative. Mookodi was installed in late 2021, commissioned, and incorporated into the IO project in a robotic queue-scheduled mode throughout 2022. Although the robotic queue-scheduled mode has been the nominal mode for the instrument since the start of 2023, it is also available (with sufficient motivation) for manual observing by astronomers to cater for a wide range of science programs. However, science programs that have so far demonstrated the system's true power and efficiency in fully automated robotic operation are those that require automated and rapid follow-up (e.g., rapid follow-up of newly discovered near-Earth asteroids, supernova follow-up via discovery reports to the TNS[5], and follow-up of alerts from the general coordinates network[17]).

In this paper, we describe the Mookodi instrument in detail. In Sec. 2, we overview the mechanical and optical design including all high-level specifications of Mookodi. In Sec. 3, we explain the software technologies behind the back-end and graphical user interface (GUI) front-end of Mookodi. We also describe the integration of the instrument into the SAAO's Intelligent Observatory project. The last part of this section briefly discusses the data reduction pipelines available to users for both spectroscopic and photometric data obtained with Mookodi. Section 4 discusses the performance, in both spectroscopic and imaging modes, of the instrument, and finally we conclude and present future plans for Mookodi in Sec. 5.

2 Design and Functionality

Experience with the Liverpool Telescope (LT) SPRAT spectrograph shows that a wavelength resolution of $R \sim 350$ and wavelength range of 4000 to 8000 Å is well suited to transient classification.[18] The same wavelength resolution and range requirements were therefore adapted for Mookodi. The Lesedi telescope has a 1-m diameter primary mirror and a final focal ratio of $f/8$, with field-correcting optics before the focal plane providing a flat focal plane. At the SAAO site, the seeing conditions are rarely below 1 arcsecond, with historical measurements suggesting a typical seeing of 1.2 arcseconds on above-average nights, implying a requirement for spatial sampling at the detector of 0.6 arcsec/pixel. Related to this, to ensure that the majority of flux is captured, we adopted a required projected slit width on the sky of 2 arcseconds but eventually settled on a stepped-slit configuration, incorporating an additional 4-arcsecond wide slit portion as well.

In addition to the spectroscopic requirements, it was also desired to use Mookodi as an imager on the telescope. This mode of operation supports both the acquisition of the target onto the spectrograph slit and a requirement for photometric scientific use. The optical field of view required was influenced by the need in both cases to have a field of view sufficiently large that suitable photometric and astrometric comparison stars would be available in relatively short exposure times (10 s) to allow these requirements to be met. We made an estimate of this by calculating the minimum field of view required to have at least five comparison stars brighter than magnitude $V = 15$ at the galactic poles, where stellar number densities are the lowest. Based on the number counts presented by Allen,[19] we found a mean density of 0.05 such objects per square arcminute, leading to a field of view requirement of 10×10 arcmin. To achieve this with spatial sampling of 0.6 arcsec/pixel implies the need for a detector with at least 1000×1000 pixels. Such a detector will also have sufficient pixels to support the desired wavelength range of 4000 Å at the required spectral resolution of $R = 350$. The detector selected for Mookodi (Andor iKon-M 934) was therefore with 1024×1024 pixels of size 13 microns.

The resolution of a spectrograph is calculated via the following equation:

$$R = \frac{0.12\rho W}{sD}, \tag{1}$$

where ρ is the grating lines per mm, W is the beam width in mm, s is the projected (on sky) slit width in arcsec, and D is the telescope diameter in meters. Adopting the requirements outlined above in combination with a requirement to use a commercial off-the-shelf volume phase holographic (VPH) 600 line/mm grating as a dispersing element, it was therefore determined that a minimum collimated beam diameter of 10 mm was required, corresponding to a collimator focal length of at least $\sim$80 mm.

The Mookodi optical design concept was adapted from that of the SPRAT spectrograph, which is deployed on the 2.0 m $f/10$ LT.[20] Both designs use the same high efficiency 600 lines/mm VPH grating as the dispersing element. The grating is sandwiched between two 10-deg BK7 wedge prisms to ensure that the input angle to the VPH is optimal for the system throughput and that the output angle yields a straight-through optical path for the imaging mode.

Detailed optical design of the system was carried out using the LENSFORGE software package. The faster focal length of the Lesedi telescope compared with LT made the optical design of the collimator a little more challenging than with SPRAT. The simple use of a field-lens plus two-element achromat collimator lens as per SPRAT was found to have a poor image quality and suffer from excessive field curvature. The final design was based on a symmetrical pair of two-element achromats to form an aplanat similar in design to the historical "rapid rectilinear" camera lens. The design uses off-the-shelf lenses and has a focal length of 91 mm (slightly in excess of the minimum of 80 mm); it allows the pupil to be located at the grating location without the use of a field lens.

To accommodate the whole spectral range on the detector, the required camera lens focal length was calculated as 50 mm. An off-the-shelf Nikon 50-mm $f/1.4$ camera lens was therefore selected for this component as a much lower cost alternative to a bespoke design of such a fast optic. The combination of a 91-mm focal length collimator and 50-mm focal length camera lens compresses the image from the $f/8$ telescope down to an $f/4.4$ image on the detector. The overall system focal length is therefore 4400 mm, and the plate scale is 21 microns/arcsec.

Each 13-micron detector pixel will therefore correspond to ~0.6 arcsec, implying that the detector will fully sample the instrument image quality and seeing as long as it is >1.2 arcsec full width half maximum (FWHM) (which is the case for most nights at the site). The wavelength dispersion will be 3.85 Å per pixel, and the imaging field of view will be 10×10 arcmin.

The design was optimized in combination with the telescope optical prescription (Table 1); a ray trace is shown in Fig. 1. The main optimization was to balance the tangential and saggital field curvature to minimize the effect of this at the flat detector focal plane and deliver optical geometric-encircled energy across the focal plane. The system also has low chromatic aberration (0.1 mm of focal plane shift between 4000 and 8000 Å) and delivers worst case (over all wavelengths) image quality of 0.2 arcsec diameter (80% encircled energy) on axis and 1.2 arcsec

Table 1 ZEMAX format prescription of the Lesedi telescope (elements 1–6), corrector optics (7–10), and Mookodi spectrograph (11–24). Note that the primary mirror has a conic constant −1.04763 and the secondary −4.894. The collimator lenses (13–18) are manufactured by Thorlabs and have an anti-reflection coating (<1% reflectivity between 4000 and 10000 Å). The grating is by Wasatch Photonics.

Number	Comment	Radius	Thickness	Glass	Semidiameter
0	Auxiliary	inf	inf		512.9911
1	Secondary	inf	1967.5680		512.3628
2	Aperture	inf	20.8316		500.0000
3	Primary	−6000.0000	−1988.4002	MIRROR	500.0000
4	Secondary	−3139.9880	1575.4600	MIRROR	181.6862
5	Flat	inf	412.9400		110.3146
6		inf	642.2975		91.6695
7	Corr L1	−1146.9260	15.0000	S-FPL53	62.7461
8		−294.6742	74.0017		62.6006
9	Corr L2	−183.0687	17.0000	F_SILICA	53.9707
10		−446.0783	50.0000		54.3581
11	Slit	inf	50.0000		52.7274
12		inf	79.5000		25.0000
13	Collimator	328.2011	4.0000	N-SF6	25.4000
14	AC508-180	115.4281	9.5000	N-LAK22	25.4000
15		−144.4444	5.0000		25.4000
16	AC508-180	144.4444	9.5000	N-LAK22	25.4000
17		−115.4281	4.0000	N-SF6	25.4000
18		−328.2011	30.0000		25.4000
19	Filters	inf	35.0000		40.0000
20	Front grism	inf	20.0000		12.0000
21	Grating	inf	20.0000		12.0000
22	Back grism	inf	5.0000		12.0000
23	Nikon 50 mm	Paraxial	50.0000		17.5000
24	Detector	inf	0.0000		9.5000
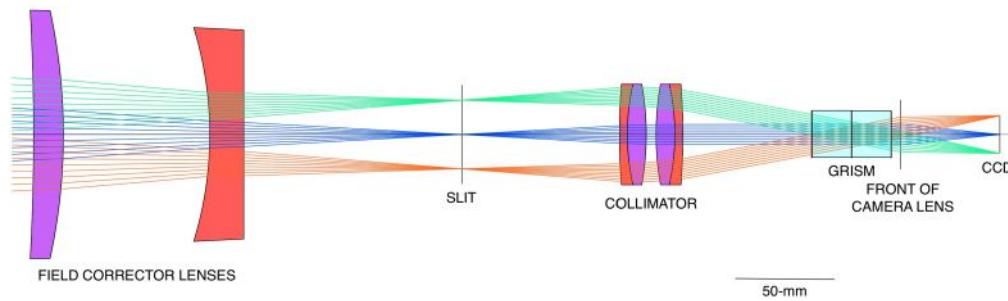
Fig. 1 Optical layout of Mookodi in imaging mode. The first two optical elements shown are the telescope field-corrector. The 50-mm Nikon camera lens is represented by a paraxial lens (vertical line) in front of the detector. When deployed, the slit is located at the telescope focus, and the grating is at the system pupil between the collimator and camera lenses.

diameter (80% encircled energy) at the field corners. This corresponds to an off-axis FWHM of ~0.8 arcsec, below the typical site seeing. Inspection of the spot diagrams (Fig. 2) showed that the combined effects of the aberrations is fairly benign, just resulting in a fairly circular broadening of the point spread function with no strong coma or ellipticity introduced. Although no detailed tolerancing analysis was carried out, simple tests showed that decentering the spectrograph with respect to the optical axis of the telescope introduced no more than 0.1 arcsec additional encircled energy per mm offset and that even gross offsets of 5 mm of the various optical components within the spectrograph itself had a negligible effect.

Provision was also made in the optical design for a set of filter slides (maximum total thickness 35 mm) between the collimator and the grism assembly to be placed as close as possible to the grism. These host an order blocking filter (4000 Ålong pass) for spectroscopic mode and various imaging filters, as described below.

Figure 3 shows the overview CAD render of the instrument showing the main components labeled roughly left to right.
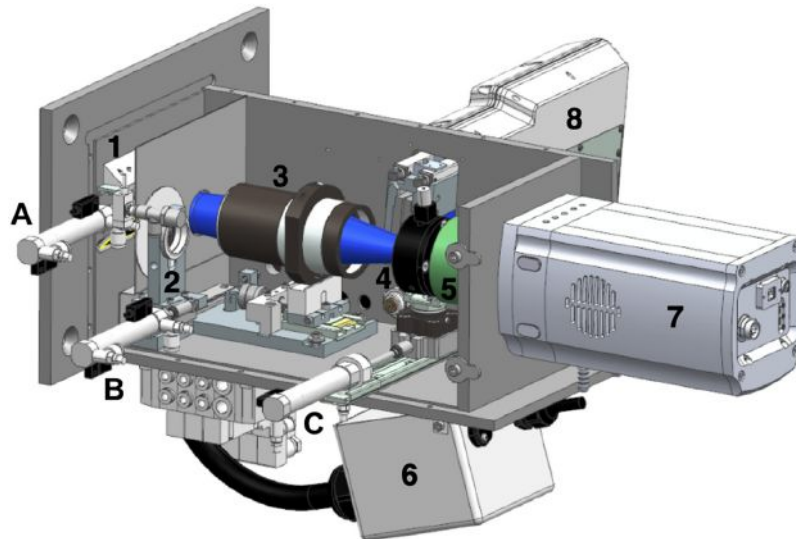
The flat/arc lamp mirror, the entrance slit, and the grism are all mounted on electronically controlled pneumatic pistons [see shafts protruding out of the page in Fig. 3 at locations (A), (B), and (C)] and therefore these items can be programmatically removed from the beam remotely, transforming the instrument into an imager within seconds. This is seamlessly possible because of the use of the grism (from Wasatch Photonics) as a dispersion element in spectroscopy mode, which avoids any deflection of the beam, i.e., the same optics used to image the spectrum on the detector can be used to image the telescope's native imaging plane (at the slit) without repositioning any of the optics. The Andor camera images $\sim 10 \times 10$ arcminutes^2 on sky at a plate scale of 0.59 arcsec/px in 1×1 binning imaging mode. The quantum efficiency (QE) curve of the camera is shown in Fig. 4, and further specifications of the camera are given in Table 2. The imaging mode is used for target acquisition on the slit (see Sec. 3), but the inclusion of a filter slide mechanism that contains a slide populated with a full Sloan Digital Sky Survey (SDSS) filter set allows the imaging mode to also function as a multi-filter photometric imager for science acquisitions. The SDSS filters were purchased from Asahi Spectra, and the transmission curves supplied by the manufacturer are shown in Fig. 4. The multi-filter imaging capability and respectable field-of-view of the instrument is demonstrated by the color composite image shown in Fig. 5.

When in spectroscopy mode, the entrance slit, which consists of a stepped slit (section 1: 2 arcsec $\times \sim 6$ arcmin and section 2: 4 arcsec $\times \sim 1$ arcmin), and the grisms are pneumatically moved into the beam. Specifications of the instrument when in spectroscopy mode are summarized in Table 2.

Calibration frames (arcs and lamp flats) can be taken by also moving an arc/flat lamp mirror into the beam, which feed light from two lamps housed inside a unit mounted underneath the instrument [Fig. 3(6)], via an optical bundle, onto the slit. The arc and flat lamp can be switched on/off independently but use the same optical bundle. Example arc and spectrum frames with the corresponding acquisition frame are shown in Fig. 6. The location of the stepped slit is also shown as an outline on the acquisition frames.
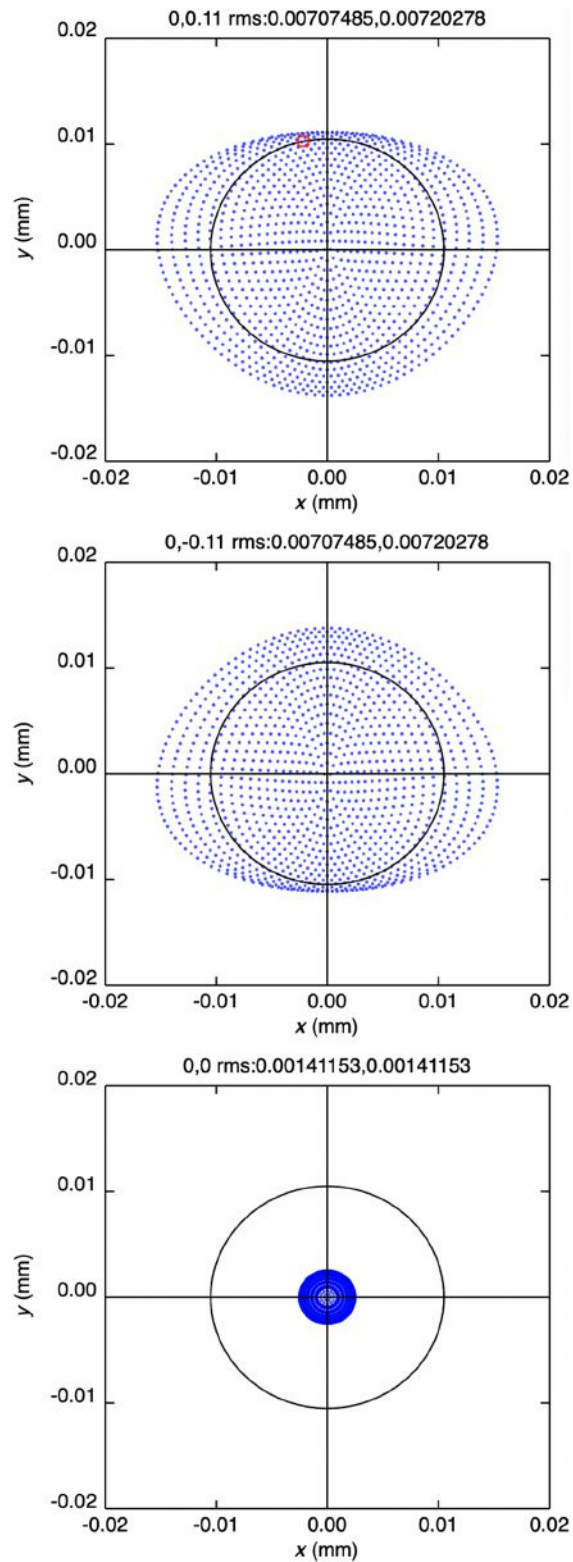
Fig. 2 Spot diagrams at 6000 Å at the field edges (top and middle) and field center (bottom). Axes are physical dimensions at the detector focal plane. The circle indicates a 1 arcsec diameter on the sky.

Fig. 3 The overview CAD render of the instrument showing the main components labeled as (1) the flat/arc lamp mirror, (2) the entrance slit of the spectrograph, (3) the collimator lens assembly, (4) the VPH transmission grating and prism pair assembly (i.e., the grism), (5) the re-imaging lens, (6) the housing for the arc and flat lamp, (7) the detector camera, and (8) the filter slide housing. The pneumatic pistons that can actuate the flat/arc lamp mirror, the slit, and the grism in/out of the beam are labeled (A), (B), and (C), respectively.
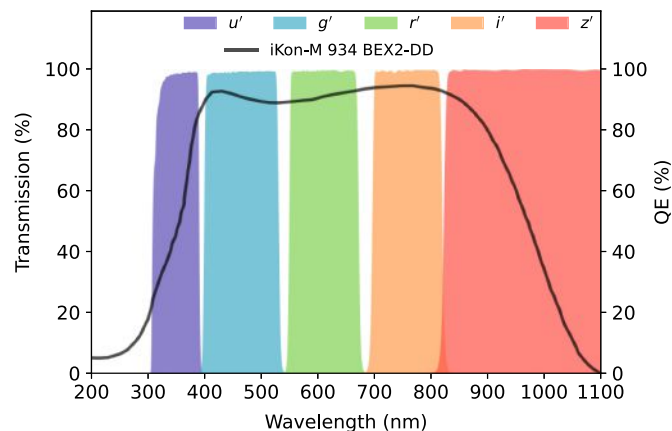
Fig. 4 Plotted in solid black is the QE curve of the Andor iKon-M 934 (BEX-DD) camera together with the transmission curves of the SDSS filters of the Mookodi instrument.

3 Software

The general software architecture that we chose for Mookodi and the Lesedi telescope (and all other instruments and telescopes that will be incorporated into the IO) is distributed, modular, and layered. The modular nature means that individual components can be developed separately and allows for individual modules to be replaced without affecting the rest of the system. A layered architecture allows for the separation of concerns; for example, higher layers do not need to be concerned about implementation details of lower layers. The distributed nature means that individual hardware components and services do not need to be co-located.

3.1 Back-End Software

The Mookodi back-end software comprises drivers for the camera and opto-mechanic hardware. The functionality offered by the drivers is made available by wrapping the drivers in TCP/IP server software that runs on Mookodi's control PC and makes the functions provided by the drivers available over the network. Client software is then able to access these functions,

Table 2 Instrument detail and specifications summary.

	Specification/Detail
Detector	Andor iKon-M 934 (BEX2-DD)
	1024 × 1024 pixels @ 13 μm/px
	0.01700 e$^-$/pixel/sec @ −80°C
	127 729 e$^-$ pixel well-depth
	Read noise: 3.2 e$^-$ (slow readout - 0.05 MHz)
	13.5 e$^-$ (fast readout - 5 MHz)
	Gain: 1.2 e$^-$/ADU (high gain, slow readout)
	1.5 e$^-$/ADU (high gain, fast readout)
	Allowable exposure times: 0 to 3600 s
	Minimum readout dead-time: ~300 ms.
	(Full-frame, 2 × 2 binning, fast readout)
Spectroscopy spectral range	4000 to 8000 Å
Spectral dispersion	3.86 Å/px
Narrow slit (section 1)	2 arcsec × ~6 arcmin
Wide slit (section 2)	4 arcsec × ~1 arcmin
Spectral resolution (narrow slit)	$R = 360$ @ 4600 Å, $R = 370$ @ 6900 Å, $R = 420$ @ 7600 Å
Spectroscopy sensitivity	SNR > 5 @ 16th magnitude (1000 s)
Wavelength calib. arc lamp	Xenon Pen-Ray (Analytik Jena)
Imaging wavelength range (throughput $\gtrsim$20%)	300 to 1000 nm
Imaging field-of-view	10.06 arcmin × 10.06 arcmin
Imaging plate-scale	0.59 arcsec/px @ 1 × 1 binning
Photometric filters	Full SDSS ($u'g'r'i'z'$)
Limiting magnitude	~20.0 in r' and ~19.5 in g', i', and z' (SNR = 3, 60 s exposure, 1 × 1 binning, high gain, fast readout)

i.e., controlling the camera and opto-mechanics of Mookodi can be done from any computer connected to the network running the client software.

The camera driver allows clients to set parameters such as exposure time, readout speed, gain, and binning; allows for control of shutter behavior (always open, always closed, or automatic); and allows clients to start or stop exposures.

For efficiency reasons, the driver writes captured data directly to the disk in the form of flexible image transport system (FITS) files, and an individual FITS file is produced for each exposure. To allow system information to be recorded, the camera driver may be sent a list of such data prior to requesting an exposure. This information may include the telescope pointing information, current environmental conditions, and state of the opto-mechanic subsystem. The additional data are included alongside a set of camera-specific data in the FITS file headers.

To allow for monitoring of the camera subsystem, the driver may be queried for the camera state and can also on demand produce an array of the most recent image taken by the camera.

The optomechanical driver allows clients to switch the arc and flat lamps on or off and to move the arc/flat mirror, slit, and grism into or out of the beam. The two filter slides may be moved so that particular filters are moved into or out of the beam or that no filters are in-beam.

Fig. 5 Composite false-color image with the rgb-channels corresponding to images taken in the g'-, r'-, and i'-bands of the Pillars of Creation in the Eagle Nebula. Fifty images in each filter were stacked (20 s/exposure in i'-filter and 10 sec/exposure in g'- and r'-filter) before the color composition was created. The camera settings in all filters were high-gain and fast-readout (see Table 2 for detail). The image illustrates both the multi-filter capability and the $\sim 10' \times 10'$ field-of-view of the Mookodi instrument in imaging mode.

3.2 Front-End Software

The main mode of Mookodi is fully automated robotic observing (see Sec. 3.3), but manual observing by a human via a GUI front-end is still possible. The technology, design, and approach[22] for Mookodi's GUI is similar to that of the latest GUIs used at the SAAO's other telescopes/instruments (including the telescope control system of the Lesedi telescope that Mookodi is mounted on).

The front-end software includes client software for each of the back-end hardware components, software to integrate these, and software with which users interact. The "users" in this case may be human observers or an automatic agent.

The client software allows commands to be sent to a specific hardware component. The integration layer of the software allows for simultaneous communication with both hardware components, as well as the telescope and weather monitoring software.

An advantage of our software architecture is that multiple different interfaces may be constructed using the same underlying blocks, and in fact, these may run simultaneously. The interface provided for human users (i.e., the GUI) is a web interface, built atop the integration software. A robotic interface (described in Sec. 3.3) is built using the same underlying components and allows for scripted and automatic observations using the instrument and telescope.

3.3 Robotic Software and Integration into SAAO's Intelligent Observatory

A critical function of the Mookodi instrument for the use of robotic rapid follow-up observations is the ability to automate target acquisition on the slit. This is achieved by first determining preset "magic pixel" positions on the charge-coupled device (CCD) that correspond to desired slit locations. That is done by generating an image of the profile of the slit on the detector by back-illuminating the slit with some spatially uniform light (e.g., during a sky-flat in twilight) when the instrument is set in imaging mode and the slit is placed in the beam. This profile provides the area on the CCD corresponding to the slit entrance and pixel locations along this area (e.g., one location on the narrow part and one location on the wide part of the slit) can be identified as predetermined "magic pixel" positions on which a star has to be positioned (in imaging mode) for it to pass through the desired location along the slit (when in spectroscopy mode). These "magic pixel" locations only have to be determined once and not by means of a nightly procedure, provided the slit is repeatedly positioned at the exact same location within the beam. This position
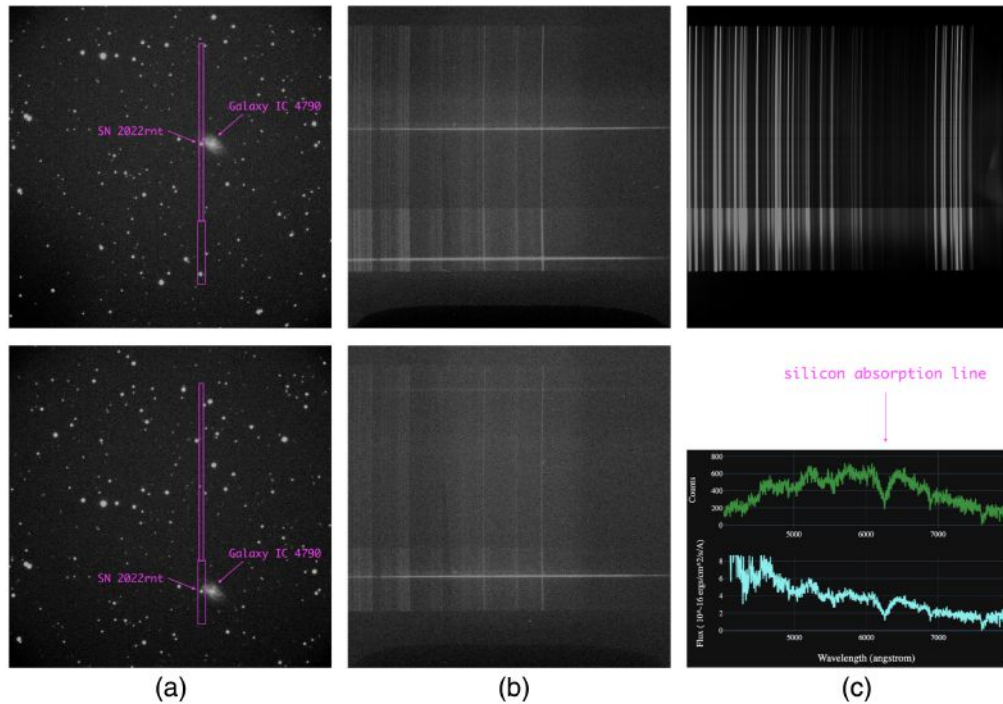
Fig. 6 Shown in panel (a) are the 4-s exposure acquisition images of the transient source SN 2022rnt discovered by the MASTER GLOBAL Robotic Net[21] in Galaxy IC 4790 (see bright source, mag ≈ 16.5, directly left of the galaxy). The pink outline shows the location of the stepped slit, with the top image showing the source positioned in the narrow region of the slit and the bottom image showing the source positioned in the wide region of the slit. The corresponding spectrum exposures are shown in panel (b) with (top) the narrow slit frame, a 10 min exposure, and (bottom) the wide slit frame, a 3 min exposure. Note that there is a subtle y-offset between the target in imaging mode and the location where the spectrum trace appears on the CCD. This discrepancy is likely attributed to a very minor tilt in the non-adjustable grism assembly, inadvertently introducing an upward deflection of the dispersed beam. However, it is important to note that this offset is constant, has no impact on performance of the instrument or analysis of the spectra, and is merely a slight inconvenience. Shown in panel (c) (top) is an example arc calibration frame that is automatically taken after each spectrum exposure. The bottom panel in (c) shows the preview spectra generated by our quick-look spectroscopy pipeline (see Sec. 3.4) of the wide-slit spectrum exposure. The distinct broad-featured silicon absorption line unique among Type Ia supernovae (the classification of SN 2022rnt) around 6200 Å is clearly present.

repeatability of the slit is ensured through a physical hard end-stop of the slit mount attached to the pneumatic piston and tested to be good within a distance corresponding to less than a pixel on the CCD.

To automate the positioning of the star on a "magic pixel," the telescope is pointed to the desired right ascension (RA) and declination (Dec) of the target (Lesedi's pointing accuracy is excellent and the target will be somewhere within the field-of-view of Mookodi in imaging mode) and then to take a short (~4 s) exposure with Mookodi in imaging mode and astrometrically calibrate the frame through a locally hosted astrometry.net[23,24] server. This server uses the Gaia DR2 index files, and the locally hosted nature of the server means that the astrometric solution results are typically returned within a few seconds. The observer-provided RA and Dec co-ordinates of the target are converted to pixel-coordinates using the astrometric solution and the offsets to the calculated "magic pixel" location. The offsets in pixels are then reconverted to offsets in arcseconds using the plate-scale (a constant value but also provided by each frame's astrometric calibration), and the telescope is commanded to "nudge" the pointing by the calculated arcseconds to eliminate offsets. A new exposure is taken to verify that the nudge was successful, and at most a second iteration of the above procedure is required to align the star on the "magic pixel." We therefore automatically do this procedure twice to be safe (see Sec. 4.3 for the position accuracy of this routine). In addition, we made an "acquire on nearest" option available

to users, which, when selected, performs an extra step of "nudging" the pointing of the telescope to position the source located closest to the input RA and Dec coordinates to the "magic pixel" location. This is useful, for example, when the reported discovery coordinates of a transient have uncertainties of a few arc seconds.

Once the required target is located on the "magic pixel," the auto-guider has to be activated. The exit port of Lesedi has a field-of-view with a diameter of about 1 deg with Mookodi grabbing the central $\sim 10' \times 10'$. The auto-guider on Mookodi, with a CCD area capturing about $2' \times 2'$, can patrol the unused semi-circular annulus area above the field-of-view captured by Mookodi via an XY translation stage. To automate the process of setting up the guider, the exact RA and Dec that the telescope is pointing at (from the "magic pixel" procedure's astrometric calibration) is used to query a locally hosted American Association of Variable Star Observers (AAVSO) Photometric All Sky Survey catalog[25] (or the Gaia catalog[26,27] via the Python Astroquery package[28] as a backup routine) for stars within the guider's range of that central RA and Dec. The guider XY translation stage's range and step-size were pre-calibrated such that the RA and Dec offset of any given star from the central RA and Dec can be converted to an X and Y position on the translation slides to which the guider can be maneuvered. Once the guider is maneuvered to the desired X and Y location corresponding to the most appropriate available guide star (to prevent vignetting of the science frame by the guide probe, we opt for a guide star located farthest from the Mookodi field-of-view that meets a specific magnitude threshold criteria.), the magic pixel routine described in the previous paragraph is repeated to ensure that the science target is in the slit in case any drift occurred during setting up the guider position (this can take up to one minute). The guider control system (now with a guide star on the guider's detector and the science target in the slit) is then immediately activated. Section 4.3 discusses the performance of the guider once it is active.

To schedule automated observations on Mookodi, the SAAO has opted to employ tried-and-tested technology and use the recently open-sourced Observatory Control System (OCS) software[29] developed by the Las Cumbres Observatory (LCO). The LCO's OCS is also already Astronomical Event Observatory Network (AEON) compatible, which is extremely attractive for the SAAO's IO project. AEON will be a collection of world-class telescope facilities that can be accessed on demand, specifically aimed at rapid follow-up of discoveries in the era of LSST-like surveys. Mookodi is the first SAAO instrument to be implemented on the SAAO's version of the OCS, but in the future many more will be implemented. Observation requests are submitted to the OCS (either manually through a completed web-form or programmatically with the API provided), and the OCS schedules all requests into a dynamic observing queue that can change (rearranged or pre/appended) at any point as new requests are submitted. A continuously running "poller" on the observation control PC requests the latest queue with requests assigned to Mookodi every minute and executes the request at the top of the queue (unless that request is already in progress) by converting the observation request details into commands that our developed back-end software for Mookodi and the telescope can handle.

3.4 Data Reduction Pipelines

There are two data reduction pipelines recommended for the users. Both are independently developed but publicly available and open source, which allows for further development and/or implementation of instruments other than the initial instrument for which it was developed. The first is the automated spectrophotometric reduction (ASPIRED) pipeline[30] for Mookodi spectroscopy data. Although the pipeline is designed for common use on different instruments, a Mookodi-specific example-code and instruction pack is available for users to download.[31] The pipeline can perform cosmic ray removal, polynomial trace fitting, and flux calibration. Example spectra extracted using ASPIRED are shown in Figs. 7 and 8.

For Mookodi photometry data, we support and provide a download link with user instructions[32] for a modified "SAAO-version" of the TEA-Phot pipeline[33] that was developed specifically for high-cadence ground-based photometry. The pipeline can deliver optimized differential light curves of a single source in the frame using a single comparison star. The pipeline is Python based and fully open source, which allows users to easily do further development/modifications for their needs. The time-series light curves from the time-stamping test-observations at the end of Sec. 4.4 were generated using TEA-Phot.
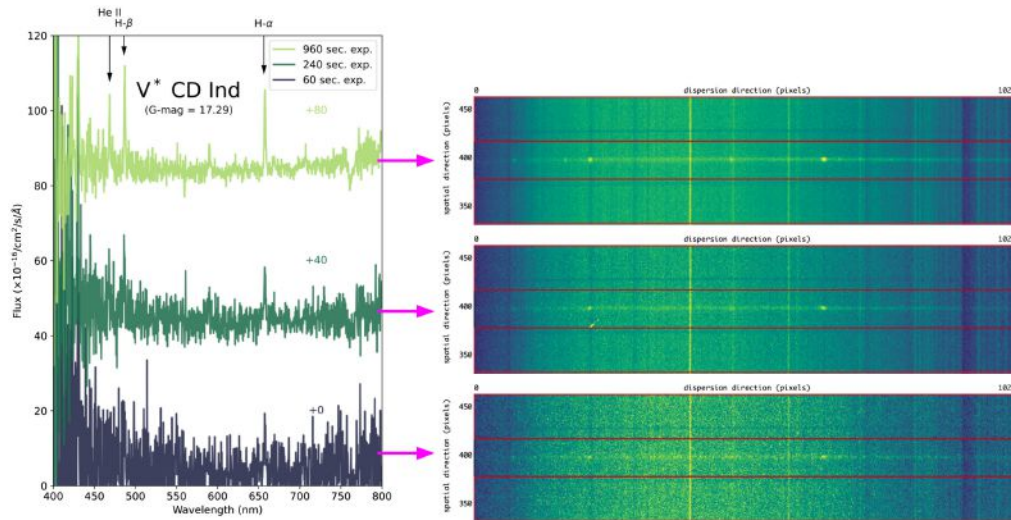
Fig. 7 Faint object example: shown on the left are flux calibrated spectra of V^* CD Ind, a Cataclysmic Binary, extracted from the science exposures using ASPIRED. The upper two spectra are vertically displaced, for display purposes. This target has a Gaia G-band magnitude of 17.29 with clear Balmer emission lines present. The spectra were taken with the source in the narrow-slit and camera settings on high-gain and slow-readout (see Table 2 for detail). Spectra were taken with the moon illumination at 97% and separation between the target and the moon of 41 deg. The airmass at the time of the observation was 1.36. Shown on the right are cutouts from the science exposure frames illustrating the trace detection and extraction done by ASPIRED for the 16 min (top), 4 min (middle), and 1 min (bottom) exposure.
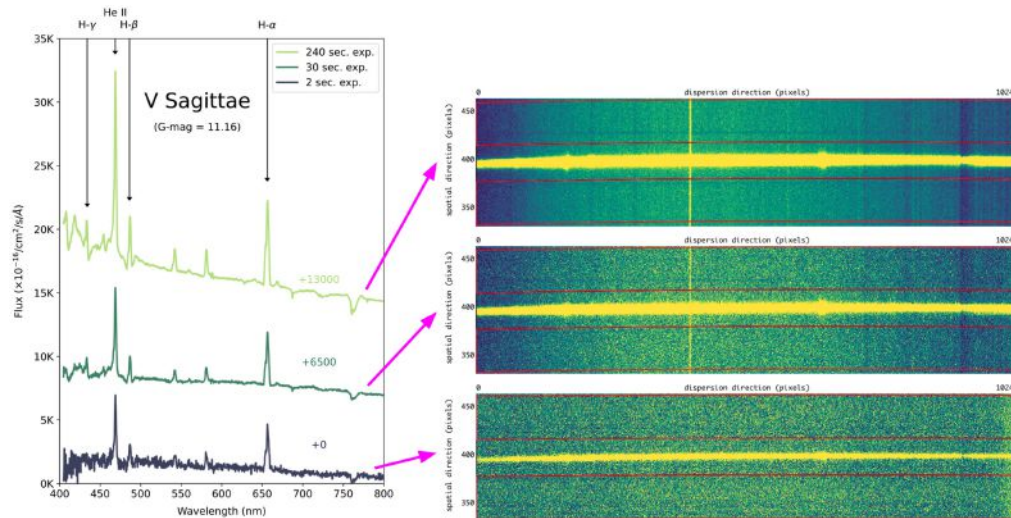
Fig. 8 Bright object example: shown on the left are flux calibrated spectra of V Sagittae extracted from the science exposures using ASPIRED. The upper two spectra are vertically displaced, for display purposes. This target has a Gaia G-band magnitude of 11.16 with clear Balmer emission lines present. The spectra were taken with the source in the narrow-slit and camera settings on high-gain and slow-readout (see Table 2 for detail). Spectra were taken with the moon illumination at 86% and separation between the target and the moon of 39 deg. The airmass at the time of the observation was 1.69. Shown on the right are cutouts from the science exposure frames illustrating the trace detection and extraction done by ASPIRED for the 240 s (top), 60 s (middle), and 2 s (bottom) exposure.

In addition, we developed two quick-look Web-GUI user interfaces, using the same technologies as our Web-GUI front-end software for the instrument, which enable users to preview spectra of spectral data and light-curves of photometry data immediately after the image files are saved to disk. The quick-look data also enable users to preview archival data. The quick-look

pipeline for spectroscopy does not use ASPIRED. Instead, the pipeline uses a simple spectral extraction routine, written in Python, and pre-calculated wavelength and flux sensitivity functions for calibration. For the latter, it uses archival flux standard star spectra and arc lamp exposures, so those frames are not required to preview the data with approximate wavelength and flux calibration. The spectrum plot shown in Fig. 6(c) was generated using the quick-look pipeline. The quick-look photometry pipeline uses TEA-Phot on the back-end.

4 Performance

4.1 Spectroscopy

Using the ASPIRED pipeline, which can provide dispersion solutions using arc spectra, the spectral resolution of Mookodi and the spectral performance along the slit length were established. Figure 9 summarizes the spectral resolution result at the center (along the slit) of the narrow slit: the spectral resolution is $R = 363$ at 463 nm, $R = 374$ at 688 nm, and $R = 423$ at 764 nm. The spectral resolution (i.e., emission line-width) along the slit remains constant, and the achieved spectral resolution compares favorably with the design resolution of $R \approx 350$.

Because Mookodi is mounted on a Nasmyth port of an alt-azimuth telescope with a field-derotator, the instrument experiences a changing gravity vector during a track. Any flexure in the instrument during a potentially long spectroscopy exposure (e.g., 20 min) could introduce loss of spectral resolution or inaccurate spectral calibration. To determine the maximum amount of flexure possible, arc spectra were taken at two extreme rotation angles. For the first angle, the gravity vector was positive along the spectral dispersion axis of the instrument (derotator angle of 90 deg), and the second derotator angle was negative to the spectral dispersion axis (derotator angle of -90 deg). The median shift in emission line positions along the spectral axis at these two extreme derotation angles was less than a pixel and was measured to be approximately 0.1 nm. Therefore, we conclude that there is negligible flexure present in the instrument.

To determine the throughput of the instrument, we observed a spectrophotometric standard star and compared it with the flux density of the same star observed by Cerro Tololo Inter-American Observatory (CTIO) facility[34,35] and provided by European Southern Observatory (ESO) via their online standard stars catalog.[36] First, the Mookodi observation was reduced to a spectrum in units of counts per second using the ASPIRED pipeline. Using the Planck–Einstein relation and Eq. (2), the Mookodi spectrum was converted to flux density taking into account the surface area of the Lesedi telescope (A), the exposure time used for the observed standard (t), and the gain setting (G) of the Andor camera:

$$f_{\text{counts}} = \frac{f_\lambda \cdot A}{t \cdot G \cdot E}. \tag{2}$$

The throughput was then determined as the ratio between the Mookodi spectrum and the ESO spectrum after the wavelength bins for the Mookodi spectrum were resized to match the ESO spectrum. The result is plotted in Fig. 10 and accounts for all losses in the system including losses in the Lesedi telescope itself. The calculated throughput falls 20% to 30% short of the
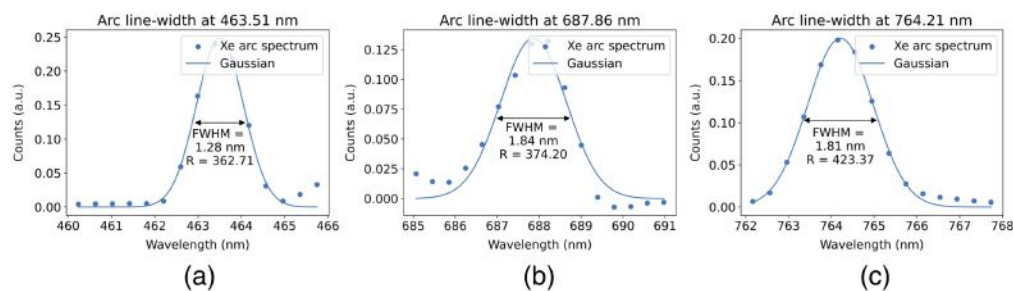
Fig. 9 Measured spectral resolution using the extracted line-width of emission lines of an arc spectrum that was calibrated using a dispersion solution generated with the ASPIRED pipeline. The line-with and spectral resolution using emission lines at (a) 463 nm, (b) 688 nm, and (c) 764 nm were determined to be 1.3 nm ($R = 363$), 1.8 nm ($R = 374$), and 1.8 nm ($R = 423$), respectively.
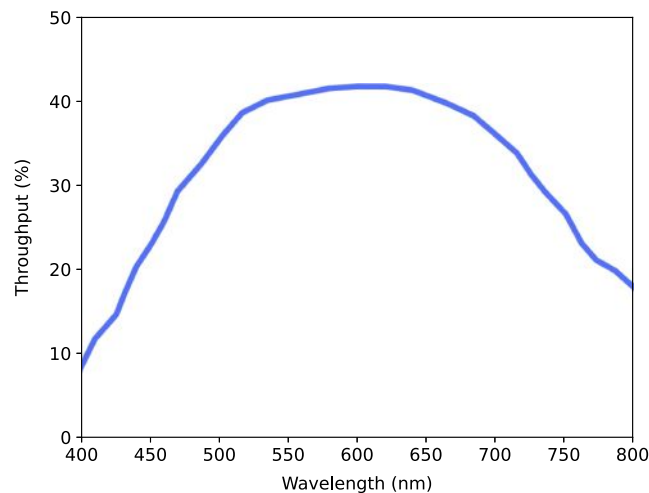
Fig. 10 Plotted is the measured throughput of Mookodi in spectroscopy mode using the ratio between a spectrum of a standard star (CD-34 241) observed with Mookodi and calibrated flux density of the same star observed by the CTIO facility[34,35] and provided by the European Southern Observatory (ESO). The observations were taken at an airmass of 1.06.

predicted values in the design simulations. However, a comparison analysis of star observations conducted with Mookodi in imaging mode and Sibonise (the alternative imager situated on the opposite Nasmyth port of Lesedi) on the same night indicates that the discrepancy is not attributed to any deficiencies in the imaging optics (the collimator or camera lens) of the Mookodi instrument. Further investigation through a comparison of star counts with another 1-m telescope on-site, during the same night and observing the same source, suggests a ~20% loss occurring somewhere within the Lesedi telescope. This potential explanation aligns with the calculated throughput deficiency. The investigation into this throughput loss within the telescope optics is currently underway.

4.2 Imaging

Astrometric calibration of images taken with the instrument in imaging mode reveal a field-of-view and plate scale of 10.06 arcmin × 10.06 arcmin and 0.59 arcsec/px (at 1 × 1 binning), respectively. By performing several focus sweeps in all filters at various ambient temperatures and extracting optimal focus positions of the secondary mirror on the telescope, the telescope focus is also automatically adjusted using a focus versus temperature look-up table when the filter is changed. This auto-focus routine via a look-up table allows us to achieve measured PSF values (FWHM) in all filters between 2.5 and 2.9 pixels (FWHM), which equates to 1.5 to 1.7 arcseconds, without any manual focus adjustments, when the independent seeing-monitor on site was reporting similar seeing values. Therefore, the optical design and this auto-focus routine meets Nyquist sampling under the typical seeing conditions at Sutherland of ~1.5 arcseconds.

Measured signal-to-noise ratio (SNR) versus exposure times in $g'r'i'z'$ for stars ranging between 11'th and 20'th magnitudes are shown in Fig. 11. The limiting magnitude (criteria: SNR > 3) with a 60 s exposure (at 1 × 1 binning, high-gain, fast-readout, see Table 2 for detail) is ~20 for the r' filter and ~19.5 for the g', i', and z' filters. The camera settings for the SNR results shown in Fig. 11 were high-gain and slow-readout (see Table 2 for detail). The observations were taken on a clear photometric night with the moon illumination at 58% and separation between the observed field and the moon of 83 deg. The airmass and the reported seeing at the time of the observations varied between 1.3 and 1.6 and 1.3 and 1.5 arc-seconds, respectively.

4.3 Target Acquisition and Position Preservation

One of the key performance requirements for fully automated spectroscopy observations is the ability to reliably position the target on the slit and thereafter maintain that positioning for several minutes.
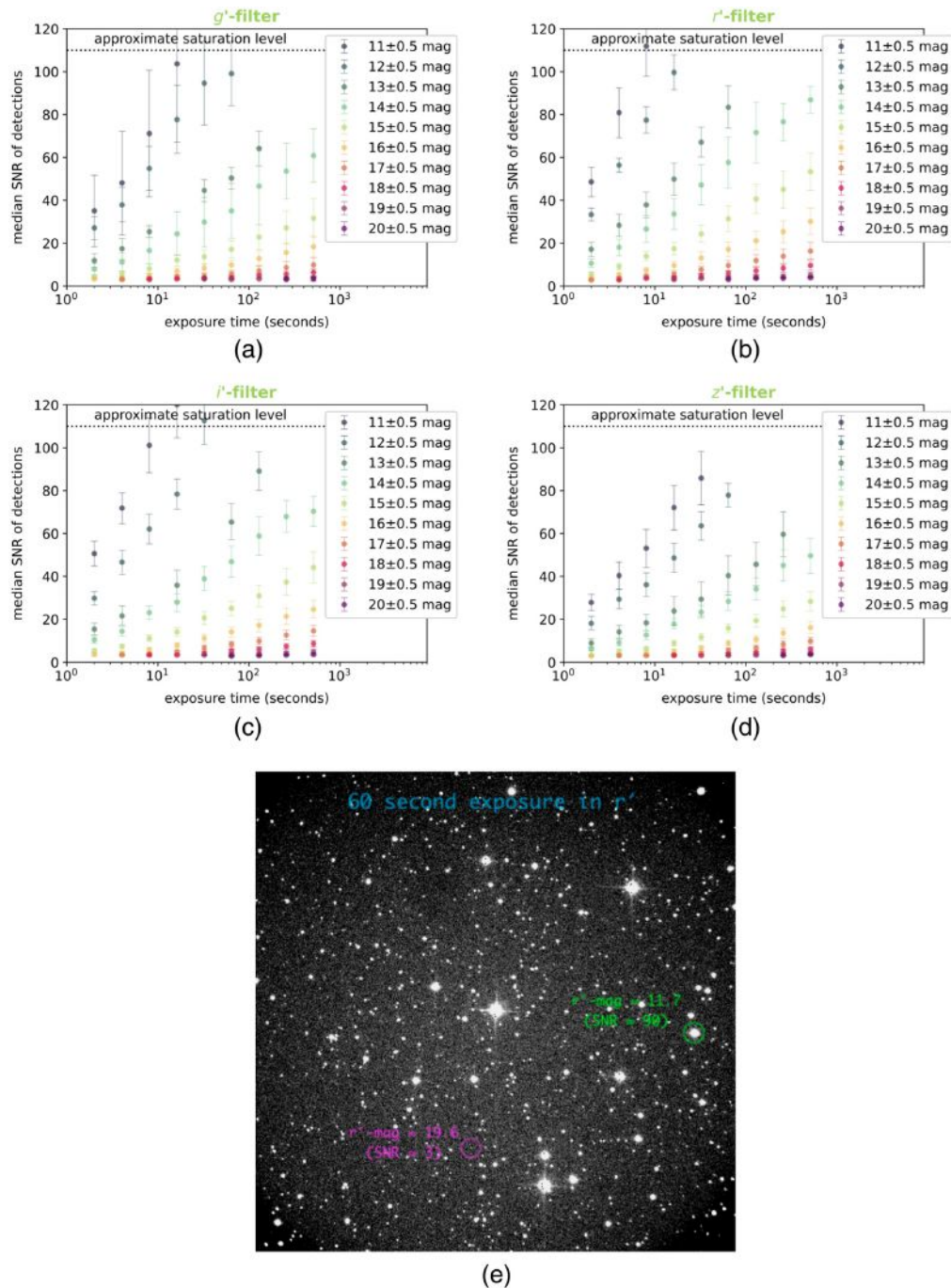
Fig. 11 Measured SNR versus exposure time for several magnitude ranges in (a) the g' filter, (b) the r' filter, (c) the i' filter, (d) the z' filter, and (e) the star field (center coordinate RA = 11:59:40.76 and Dec = −50:02:40.43) showing the stars used to calculate the SNR values shown in plots (a)–(d). This specific frame was the 60-s exposure in the r' filter. The star on the right edge circled in green is just under saturation level and has a r'-magnitude of 11.7. The star in the center lower-half of the frame and circled in pink has an SNR of ∼3 (i.e., just visible by eye) and a r'-magnitude of 19.6.

To test the reliability of positioning the target on the slit, we performed 30 individual attempts to take a spectrum of the same source, which required positioning the source on the "magic pixel" for each attempt using the routine explained in Sec. 3. Plotted in Fig. 12 is the difference between the extracted x- and y-pixel locations of the target source in the acquisition frame (i.e., the frame taken before the spectrum exposure) and the preset "magic pixel" location corresponding to the center of the slit. The plot shows that, on average, we successfully place the
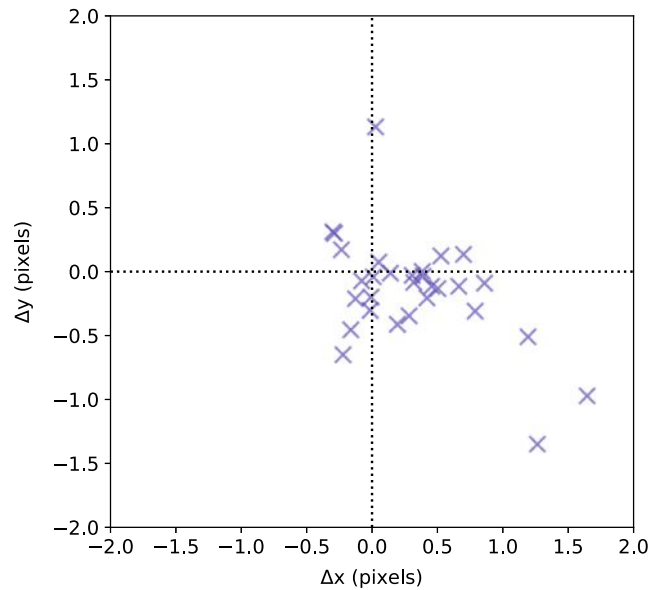
Fig. 12 Plotted is the difference between the extracted *x*- and *y*-pixel location of the target source in the acquisition frame (i.e., the frame taken before the spectrum exposure) and the preset "magic pixel" location corresponding to the center of the slit. The plot shows 30 individual attempts to place the same source on this "magic pixel" using the routine explained in Sec. 3.

source within 0.5 pixels (which equates to 0.3 arcseconds) of the desired pixel for 70% of the attempts. At worst and for only 10% of the attempts, we miss the magic pixel by 1 to 1.5 pixels (which equates to 0.6 to 0.9 arcseconds), which means that, for a small fraction of observations, ~50% of the photon flux for those spectra exposures can be lost if the 2-arcsecond narrow part of the slit is used. Therefore, for observers utilizing the robotic mode, in which capturing all flux is essential (e.g., for faint objects or absolute flux calibration), we strongly recommend utilizing the wider section of the slit, measuring four arcseconds [see Fig. 6(a) for an example of a source positioned on the narrow and wide parts of the slit].

Another performance requirement for the instrument is the on-sky position preservation. This is extremely important for spectroscopy to maintain the target position on the slit for the duration of a spectrum exposure (which is usually several minutes) but also for some long time-series observations in which observers might require the target and reference stars to remain on the same location of the CCD for the entire observation (which can span hours). Although the tracking of the Lesedi telescope is excellent, for sub-arcsecond position preservation, auto-guiding is required. Plotted in Fig. 13 is the difference between the CCD center pixel's calculated RA and Dec coordinates (via an astrometry.net astrometric solution) for each frame relative to the first frame of 127 continuous exposures taken over the course of ~4 h at 90 s per exposure. The plot shows that the auto-guider was able to maintain the telescope pointing accuracy to a standard deviation of 0.26 arcseconds in RA and 0.23 arcseconds in Dec for several hours. Those values are <15% at the narrowest slit width of 2 arcseconds, so the position preservation should be sufficient for the more stringent spectroscopy requirement for even longer (>30 min) exposures.

4.4 Time-Stamping of Exposures

A niche science domain of the SAAO's astronomer community is fast time-series photometry. Mookodi's main functionality is spectroscopy, but a frame rate of up to 2 FPS is possible (e.g., 200 ms exposure time with ~300 ms dead-time, full-frame, 2×2 binning, and fast read-out mode enabled) to serve some of this type of science. For this use, accurate time-stamping of at least half of the minimum sensible exposure time is required, and although Mookodi's exposures are not directly triggered by GPS time-triggers, as with some of our other time-series imagers, the control computer of Mookodi has its CPU clock kept accurate using network time protocol, which synchronizes the CPU clock every ~30 sec. The time stamps in the headers of all image files are obtained from the CPU clock. To test the accuracy of this time-stamping
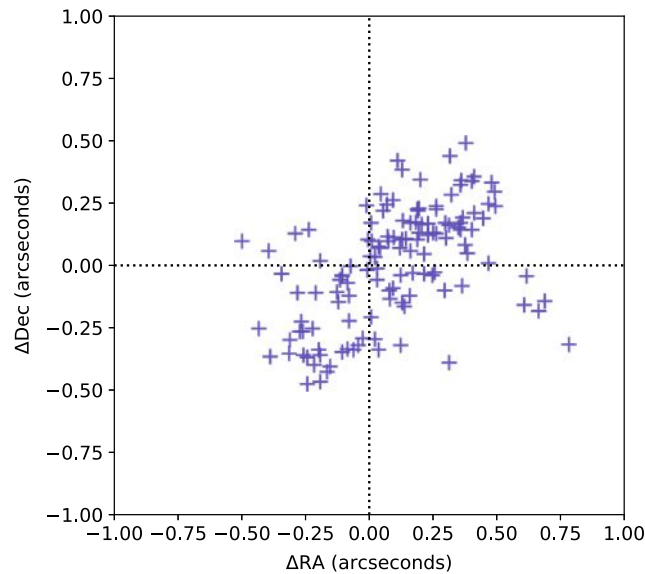
Fig. 13 Plotted is the difference between the CCD center pixel's calculated RA and DEC coordinate (via an astrometry.net astrometric solution) for each frame relative to the first frame of 127 continuous exposures taken over the course of ~4 h at 90 s per exposure with the auto-guider activated. The plot shows that the auto-guider was able to keep the telescope pointing accuracy to a standard deviation of 0.26 arcseconds in RA and 0.23 arcseconds in Dec.

approach, we make use of a procedure prescribed by Project Pluto,[37] which entails observing a fast-moving Global Navigation Satellite Systems satellite that has a very accurately known sky-coordinate for a given time. Comparing the observed sky-coordinate of the satellite in the images (after doing astrometric calibration) with the predicted sky-coordinate of the satellite at the respective time stamp recorded in the image header (and knowing the sky-rate of the satellite), it is possible to determine the accuracy of the time stamps in image headers using the offset in arcseconds and the sky-rate of the satellite in arcseconds/sec. Using this method, we were able to determine that the time-stamping of our exposures is conservatively accurate to within 80 ms. The actual performance may be better than this, as the accuracy of our test was limited by a combination of the exposure time (100 ms), the sky-rate of the satellite (30.55 arcseconds/s), the plate-scale at 2×2 binning (1.2 arcseconds/pixel), and the ability to determine the center point of the ~3 pixel streak of the satellite trail still present in a 100 ms exposure. To ensure a sensible duty cycle exceeding 50% and considering the camera's minimal achievable dead time of 300 ms (2×2 binning, fast readout), the minimum sensible exposure time for Mookodi is ~300 ms. Therefore, a time-stamping accuracy with an upper limit of 80 ms is sufficient for the fastest science programs that Mookodi can accommodate.

As an additional test, we performed simultaneous time-series observations of the binary pulsar, AR Scorpii, with Mookodi (on the Lesedi telescope) and one of the Sutherland high-speed optical cameras[38] (SHOCs, mounted on the SAAO's 40-inch telescope), which are the current work-horse cameras for the SAAO's transient/variable community. AR Scorpii displays a 3.56 h period close binary (partially covered in the simultaneous light-curves of Mookodi and SHOC shown in Fig. 14), pulsing in brightness with a period of 1.97 min.[39] The inset plot in Fig. 14, which is a cut-out of roughly 4 min of the full observation, clearly shows the faster ~2 min period. It also shows the commensurate data of the independent Mookodi and (GPS triggered) SHOC datasets, giving further confidence in the time-stamping of Mookodi.

5 Conclusion and Future Plans

We have presented Mookodi, a low-resolution spectrograph with multi-filter and fast imaging capabilities that was designed and built by the Astrophysics Research Institute of LJMU with design input from the SAAO's instrumentation division. The auto-target acquisition functionality and integration of the instrument into the SAAO's Intelligent Observatory program makes this
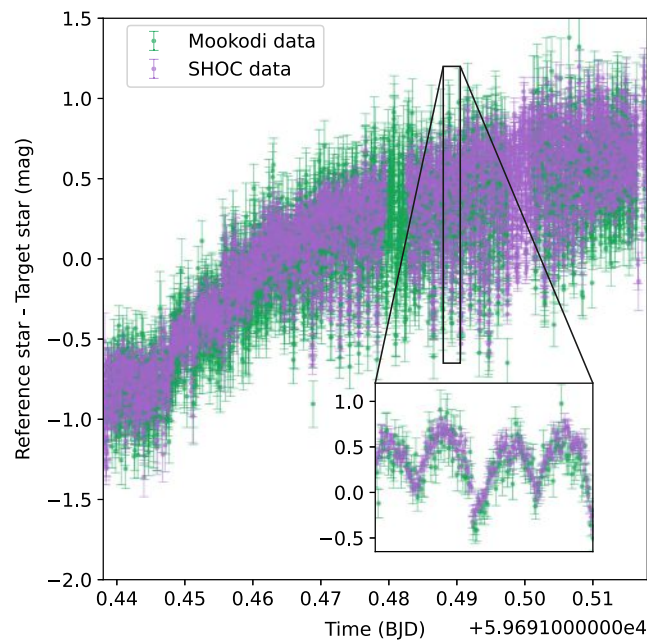
Fig. 14 Comparison of example fast-photometry data between Mookodi in imaging mode and one of the SHOCs,[38] which are the current work-horse cameras for the SAAO's transient community. Both datasets are in r'-band with exposure time for both instruments set to 1 s with ~300 ms dead-time between Mookodi exposures (negligible dead-time for the frame-transfer SHOC CCD). Both light-curves were extracted using the TEA-phot pipeline (see Sec. 3). The photometry is of the binary pulsar, AR Scorpii, that displays a 3.56 h period close binary (partially covered in the displayed Mookodi/SHOC observation), pulsing in brightness with a period of 1.97 min.[39] The inset plot, which is a cut-out of roughly 4 min of the full observation, clearly shows the faster ~2 min period. The median apparent magnitude of AR Scorpii in r'-band is ~14.4. No magnitude offsets were applied to the two data sets, but the same reference star was used, so the matching differential magnitude between the two datasets is expected.

instrument ideal for (but not limited to) quick-reaction astronomical observations, e.g., finding optical counterparts to Gamma-ray bursts, spectral classification of uniquely discovered supernova, and astrometric/photometric/spectral follow-up of uniquely discovered near-Earth asteroids.

In the future, we plan to use the derotator of the telescope's Nasmyth port that houses Mookodi to incorporate the functionality of aligning the slit to any arbitrary sky angle for spectroscopy exposures. This would allow users, for example, to align the slit along the parallactic angle, orientate extended objects to the desired geometry along the slit, or orientate the slit to locate multiple stars in the slit at the same time.

We also hope to implement a fully automated photometric pipeline that will automatically astrometrically and photometrically calibrate all sources detected in the science frames immediately after the frames are taken. This would allow for quick access to calibrated photometry to the users of any source within the frame and would support the rapid-response characterization of astronomical transients that we hope to achieve with Mookodi.

Code and Data Availability

Some of the code used to generate the results and figures is available in a publicly available Github repository, and the remainder of the code and data used to generate the results and figures is available on request from the main author.

Acknowledgments

References

1. N. Kaiser et al., "The Pan-STARRS wide-field optical/NIR imaging survey," *Proc. SPIE* **7733**, 77330E (2010).
2. G. Gilmore et al., "The Gaia-ESO Public Spectroscopic Survey: Motivation, implementation, GIRAFFE data processing, analysis, and final data products," *Astron. Astrophys.* **666**, A120 (2022).
3. R. M. Smith et al., "The Zwicky transient facility observing system," *Proc. SPIE* **9147**, 914779 (2014).
4. J. L. Tonry et al., "ATLAS: a high-cadence all-sky survey system," *Publ. Astron. Soc. Pac.* **130**, 064505 (2018).
5. IAU Supernova Working Group, Transient Name Server, https://www.wis-tns.org (accessed 17 April 2024).
6. IAU Supernova Working Group, "Transients statistics, skymaps and plots," Transient Name Server, https://www.wis-tns.org/stats-maps (accessed 17 April 2024).
7. SKA Observatory, Explore | SKAO, https://www.skatelescope.org/the-ska-project/ (accessed 17 April 2024).
8. LSST Science Collaborations and LSST Project 2009, LSST Science Book, Version 2.0, arXiv:0912.0201 (2009).
9. R. Fender et al., "ThunderKAT: The MeerKAT large survey project for image-plane radio transients," in *MeerKAT Sci.: On the Pathway to the SKA*, p. 13 (2016).
10. B. Stappers, "MeerTRAP: real time commensal searching for transients and pulsars with MeerKAT," in *MeerKAT Sci.: On the Pathway to the SKA*, p. 10 (2016).
11. J. JonasMeerKAT Team, "The MeerKAT radio telescope," in *MeerKAT Sci.: on the Pathway to the SKA*, p. 1 (2016).
12. S. Bloemen et al., "MeerLICHT and BlackGEM: custom-built telescopes to detect faint optical transients," *Proc. SPIE* **9906**, 990664 (2016).
13. K. Paterson, "MeerLICHT: MeerKAT's optical eye," *Proc. Int. Astron. Union* **339**(S339), 203 (2019).
14. S. B. Potter, "Towards an intelligent observatory," *An. Acad. Brasil. Ciênc.* **93**, e20201026 (2021).
15. H. L. Worters et al., "SAAO's new robotic telescope and WiNCam (Wide-field Nasmyth Camera)," *Proc. SPIE* **9908**, 99083Y (2016).
16. A. S. Piascik et al., "SPRAT: spectrograph for the rapid acquisition of transients," *Proc. SPIE* **9147**, 91478H (2014).
17. NASA, "GCN: NASA's Time-Domain and Multimessenger Alert System," General Coordinates Network, https://gcn.nasa.gov/ (accessed 17 April 2024).
18. A. S. Piascik and I. A. Steele, "Characterising the stability of the SPRAT autonomous imaging spectrograph," *Proc. SPIE* **10702**, 107022A (2018).
19. C. W. Allen, *Astrophysical Quantities, Athlone Press*, University of London (1976).
20. I. A. Steele et al., "The Liverpool Telescope: performance and first results," *Proc. SPIE* **5489**, 679–692 (2004).
21. V. Lipunov et al., "Master Robotic Net," *Adv. Astron.* **2010**, 349171 (2010).
22. C. H. D. R. van Gend et al., "Software architecture of the intelligent observatory local control unit," *Proc. SPIE* **12189**, 121890R (2022).
23. D. Lang et al., "Astrometry.net: blind astrometric calibration of arbitrary astronomical images," *Astron. J.* **139**, 1782–1800 (2010).
24. "Astrometry.net's documentation," Astrometry.net, 2012, http://astrometry.net/doc/ (accessed 17 April 2024).
25. A. A. Henden et al., "VizieR online data catalog: AAVSO photometric all sky survey (APASS) DR9 (Henden +, 2016)," VizieR Online Data Catalog, II/336 (2016).
26. Gaia Collaborationet al., "The Gaia mission," *Astron. Astrophys.* **595**, A1 (2016).
27. Gaia Collaborationet al., "Gaia data release 3: summary of the content and survey properties," *Astron. Astrophy.* **674**, 22 (2022).
28. A. Ginsburg et al., "astroquery: an astronomical web-querying package in Python," *Astron. J.* **157**, 98 (2019).
29. https://observatorycontrolsystem.github.io/.
30. M. C. Lam et al., "Automated spectrophotometric image reduction (ASPIRED)," *Astron. J.* **166**(1), 13 (2023).
31. SAAO, "Mookodi aspired example," TOPS Wiki, https://topswiki.saao.ac.za/images_topswiki.saao.ac.za/4/47/Mookodi_ASPIRED_example.zip.
32. SAAO, "Data reduction pipelines," Mookodi - TOPS Wiki, 2023, https://topswiki.saao.ac.za/index.php/Mookodi#Data_Reduction_Pipelines (accessed 17 April 2024).

33. D. M. Bowman and D. L. Holdsworth, "Adaptive elliptical aperture photometry: A software package for high-cadence ground-based photometry. I. Application to rapid oscillators observed from SAAO," *Astron. Astrophys.* **629**, A21 (2019).

34. M. Hamuy et al., "Southern spectrophotometric standards. I," *Publ. Astron. Soc. Pac.* **104**, 533 (1992).

35. M. Hamuy et al., "Southern spectrophotometric standards. II," *Publ. Astron. Soc. Pac.* **106**, 566 (1994).

36. ESO, "Index of /pub/usg/standards/ctiostan," 2007, https://ftp.eso.org/pub/usg/standards/ctiostan/ (accessed 17 April 2024).

37. Project Pluto, "Calibrating timing of astronomical images using navigation satellites," https://www.projectpluto.com/gps_expl.htm (accessed 17 April 2024).

38. R. Coppejans et al., "Characterizing and commissioning the Sutherland High-speed Optical Cameras (SHOC)," *Publ. Astron. Soc. Pac.* **125**, 976 (2013).

39. T. R. Marsh et al., "A radio-pulsing white dwarf binary star," *Nature* **537**, 374–377 (2016).

Biographies of the authors are not available.